Available online at www.sciencedirect.com
ScienceDirect
Computers and Structures 85 (2007) 446–457
Computers & Structures
www.elsevier.com/locate/compstruc

Simulation of inelastic cyclic buckling behavior of steel box sections

Murat Dicleli [a,*], Anshu Mehta [b]

[a] Department of Engineering Sciences, Middle East Technical University, 06531 Ankara, Turkey
[b] Department of Civil Engineering and Construction, Bradley University, Peoria, IL 61625, USA

Received 16 January 2006; accepted 15 September 2006
Available online 14 December 2006

Abstract

In this study, a nonlinear structural model is developed to simulate the cyclic axial force-deformation behavior of steel braces including their buckling behavior using the commercially available nonlinear finite element based software ADINA. The nonlinear cyclic axial force-deformation simulation is done for braces with box sections. However, the structural model and simulation techniques described in this study may be applicable to braces with various section types using other commercially available structural analysis software capable of handling material and geometric nonlinearity. The developed nonlinear brace model is verified using available test results from the literature. It is found that the accuracy of the shapes of the analytical hysteresis loops and the energy dissipated compared to the experimental ones is satisfactory for analysis and design purposes in practice. The developed nonlinear brace structural model is then used to study the effect of various ground motion and structural parameters on the seismic response of single story, single bay concentrically braced frames with chevron braces.

Keywords: Steel; Brace; Buckling; Cyclic; Computer simulation; Nonlinear

1. Introduction

Seismic design of steel buildings is based on design procedures [1–3] that utilize the high ductility of steel. Such design procedures involve certain structural components specifically detailed to respond to seismic forces by deforming beyond their elastic limit to dissipate the earthquake input energy. In a concentrically braced steel frame (CBF), the inelastic axial deformation of the braces forms the main mechanism that results in the dissipation of the earthquake input energy. The inelastic axial behavior of braces generally involves yielding under axial tension and inelastic buckling under axial compression. In a CBF, buckling of the brace is generally the first event in inelastic analysis. Hence, an accurate analytical simulation of the inelastic cyclic behavior of braces including their buckling behavior forms an important part of the analysis and design procedure.

Several existing phenomenological [4] and physical theory [5] models and relevant software such as SNAP-2D [6] are available in the literature to simulate the cyclic axial force-deformation behavior of braces including the effect of buckling. However, these models are very difficult to use in practice as they require numerous empirical parameters to define the effect of the buckling behavior of a particular brace on the overall response. Furthermore, such models are not capable of simulating the complex buckling behavior of the brace accurately since the simulation of the cyclic behavior of the brace, which is made of several straight and curved axial force–displacement segments, is performed using only approximate straight line segments defined by empirical parameters. Accordingly, several other analytical procedures that simulate buckling behavior of steel braces more easily and accurately have been developed and implemented in research-oriented structural analysis programs such as DYNAMIX [7] and OPENSEES [8]. However,

* Corresponding author. Tel.: +90 312 210 4451; fax: +90 312 210 4462.
E-mail address: mdicleli@metu.edu.tr (M. Dicleli).

0045-7949/$ - see front matter © 2006 Elsevier Ltd. All rights reserved.
doi:10.1016/j.compstruc.2006.09.010

these procedures are specifically coded in these programs and hence, they cannot be employed in the analysis and design of CBF using commercially available nonlinear structural analysis software which are often used for structural design purposes in the industry. For this purpose, a nonlinear structural model is developed as part of this study to simulate the nonlinear cyclic axial force-deformation behavior of steel braces including their buckling behavior using commercially available nonlinear finite element based programs. The simulation of cyclic axial force-deformation behavior is done using the program ADINA [9], which uses the linear and nonlinear solution procedures described in [10], for braces with box sections commonly used in the design of braced frame systems due to their relatively higher global buckling capacity compared to braces with other section types (e.g. T or I) having equal cross-sectional area. However, the structural model and simulation techniques described in this paper may be applicable to braces with various section types using other commercially available structural analysis software capable of handling material and geometric nonlinearity.

2. Research objectives and scope

The main objective of the presented research study is to develop a nonlinear structural model to simulate the inelastic cyclic behavior of pin-ended steel box section braces based on their global buckling and tensile behavior using commercially available structural analysis software capable of handling material and geometric nonlinearity. The secondary objective of this research study is to use the developed nonlinear brace structural model to study the effect of various ground motion and structural parameters on the seismic response of single story, single bay CBF with chevron braces.

For a pin- or fix-ended steel box section, the end boundary conditions in both orthogonal directions are the same. Thus, the buckling always takes place about the weak axis of the member regardless of the problem being two or three-dimensional. In studying the buckling behavior of steel box sections, the two-dimensional plane is assumed to be the buckling plane of the member. Thus, the findings from this two-dimensional research study are also applicable to three-dimensional buckling problems. Furthermore, the developed analytical model is intended for design purposes in practice. Thus, local buckling and low-cycle fatigue effects are kept beyond the scope of this study.

3. Inelastic cyclic axial behavior of steel braces

A physical understanding of the inelastic response of a steel brace subjected to reversed axial cyclic load is required to comprehend the modeling procedure described in the following sections.

The inelastic behavior of steel braces is generally expressed in terms of an axial load, P, an axial displacement, δ, and a transverse displacement, Δ, at the mid-point of the brace as shown in Fig. 1a [11]. A typical hysteresis curve of a brace member under cyclic axial load is illustrated in Fig. 1b [11]. Starting from the unloaded condition 0, the brace is compressed in the linearly elastic range along segment 0–1. Due to the initial imperfections within the brace, second order effects are generated under the applied axial load and the brace deflects transversely as demonstrated in Fig. 1a. Accordingly, in addition to the axial load, the brace is subjected to second order moments along its length. The largest value of the second order moment occurs at the mid-point of the brace ($P \times \Delta$) where the transverse displacement is maximum. At a critical value of the transverse displacement of the brace, the second order moment in the brace will be equal to its plastic moment capacity under the applied axial load. At this point, the buckling load (point 1) is reached. Additional increases in the axial displacement result in larger transverse displacement, Δ, because of the plastic hinge rotations at the mid-point of the brace. Consequently, the second order moment at the mid-point of the brace increases. This results in a drop in the axial force resistance of the brace along segment 1–2 due to the moment–axial force interaction effects as demonstrated in Fig. 1c. That is, an increase in second order moment from M_1 to M_2 produces a decrease in axial load capacity from P_1 to P_2. Upon unloading from point 2 to a level where the axial load is zero (point 3), the brace retains residual axial (δ) and transverse (Δ) deformations. When the brace is loaded in tension from point 3 to 4, the behavior is elastic. At point 4, the product of the axial load and transverse displacement again equals the plastic moment capacity of the brace under the applied axial load. Thus, a plastic hinge at the mid-point of the brace is produced for the second time. However, along segment 4–5, the plastic hinge rotations act in the reverse direction of that along segment 1–2 and reduce the magnitude of the transverse deflection until the yield point (5) in tension is reached.

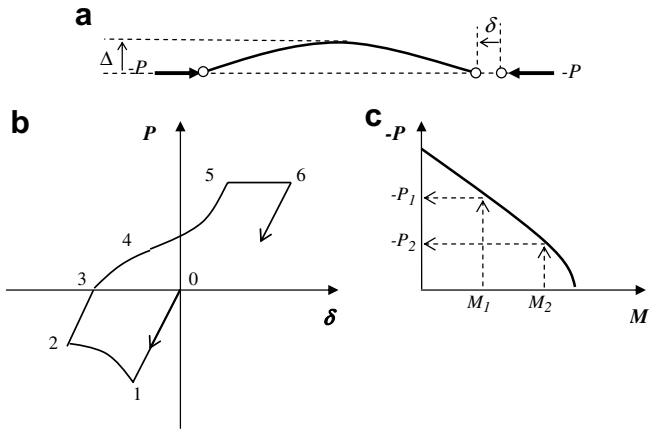

Fig. 1. (a) Displaced shape of steel brace under axial load; (b) typical inelastic cyclic behavior of a steel brace; (c) effect of increased second order moment on axial load capacity.

4. Proposed structural model and simulation techniques

A nonlinear structural model is developed to simulate the inelastic buckling behavior of steel braces using commercially available nonlinear finite element based programs. The model employs (i) large displacement analysis procedure to account for the second order effects due to the presence of axial loads and transverse deformation (Δ) of the brace, (ii) inelastic bending behavior of the brace to simulate the plastic hinge formation at the mid-point region of the brace beyond the onset of buckling (iii) inelastic axial behavior of the brace to simulate the yielding of the brace in tension.

The proposed structural model consists of a nonlinear brace member demonstrated in Fig. 2a. An initial eccentricity (imperfection or kink), e, is introduced at the centre of the brace member to produce a kinked brace element. The initial eccentricity, e, is chosen such that when the axial load reaches the buckling load, P_b, of the brace, the reduced plastic moment capacity, M_{pb}, of the brace corresponding to the buckling load, P_b, is reached at the vertex of the brace element due to second order effects (point 1 in Fig. 1b). Beyond this point, the axial load capacity of the member constantly decreases due to the combined effects of increasing second order moments and moment–axial force interaction as the member folds under the effect of the axial loads applied at the brace ends (see Fig. 1c and segment 1–2 in Fig. 1b). Accordingly, a plastic hinge region accounting for moment–axial force interaction is assumed at the vertex of the kinked brace element. The inelastic behavior of the plastic hinge region under different levels of axial loads throughout the loading history is simulated using a set of moment–curvature relationships of the brace cross-section under incremental levels of axial loads ranging between $P = 0$ and $P = 0.8P_y$ as qualitatively demonstrated in Fig. 2b, where P_y is the yield axial capacity of the brace. Furthermore, the inelastic axial stress–strain relationship of the brace is defined (Fig. 2c) to simulate its axial force-deformation relationship once the brace unfolds (segment 3–4–5 in Fig. 1b) and starts yielding at large levels of axial tensile loads (point 5 in Fig. 1b). It is noteworthy that the initial eccentricity, e, is small enough to allow for an accurate prediction of the axial force-deformation relationship of the brace under tensile/compressive axial loading. The derivation of the initial eccentricity is presented in the following section. The proposed nonlinear structural model of the brace is capable of completely producing the force–axial displacement relationship shown in Fig. 1b.

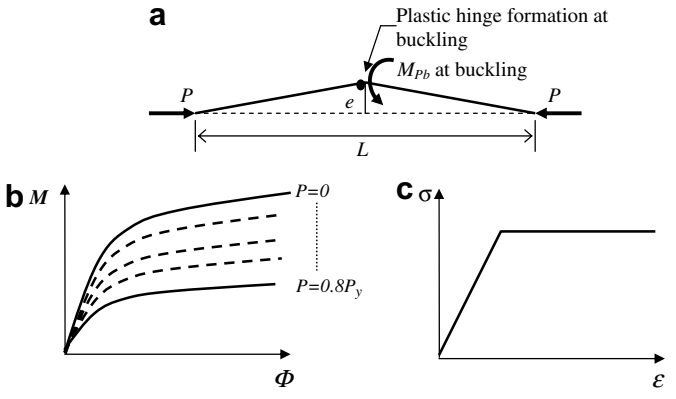

Fig. 2. (a) Nonlinear brace buckling model; (b) moment–curvature relationship of brace cross-section for incremental levels of axial loads to account for moment–axial force interaction; (c) axial stress–strain relationship of the brace.

5. Derivation of brace initial eccentricity for the model

To simulate the buckling behavior of steel braces, the value of the initial eccentricity (or kink), e, (Fig. 2a), which will result in plastic hinge formation at the vertex region of the brace element at a compressive axial load equal to the buckling load of the brace, needs to be derived by considering the second order effects. Under the application of a compressive axial load, P, and due to the presence of the initial eccentricity (or kink), e, the brace element deforms transversely by Δ_1 at its vertex due to the second order effects, $P \times e(x)$, along its length as shown in Fig. 3a. As a result, the effective eccentricity becomes $(e + \Delta_1)$. Consequently, the initial second order moments, $P \times e(x)$, along the length of the brace are further amplified by $P \times \Delta_1(x)$ resulting in an increase in the transverse deformation of the member and hence a further increase in the eccentricity (or kink) of the member. The amplification of the second order effects and brace transverse deformation continues until a final transverse displacement and force equilibrium state is reached.

To obtain the initial second order displacement, Δ_1 due to the initial eccentricity, e, first a section is cut through the brace at a distance x from the left end of the brace and the value of the eccentricity at that particular point is calculated as $\frac{2e}{L}x$ where, L is the length of the brace as demonstrated in Fig. 3b. From the static moment equilibrium of the free body diagram (FBD) of Fig. 3b, the second order moment, M, is obtained as

$$M = \frac{2Pe}{L}x. \tag{1}$$

The initial transverse deflection, Δ_1, of the brace due to the second order effects is then calculated using the unit dummy load method as [12]:

$$\Delta_1 = \int_0^L \frac{Mm}{EI}\,\mathrm{d}x, \tag{2}$$

where, m is the moment along the brace due to a vertical unit load acting at the vertex of the brace element as demonstrated in Fig. 3c and d, and E and I are respectively the modulus of elasticity and moment of inertia of the brace about the axis of buckling. From the static moment equilibrium of the FBD of Fig. 3d, the unit dummy load

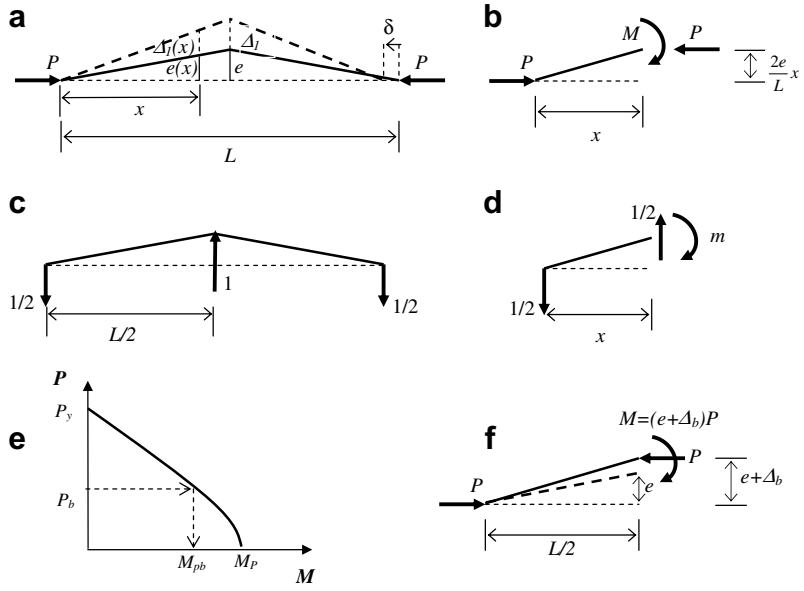

Fig. 3. (a) Effective eccentricity under axial load; (b) free body diagram of the brace to the left of section at x; (c) unit dummy load applied at the vertex of the brace element; (d) free body diagram for the unit dummy load; (e) reduced plastic moment at buckling load; (f) second order moment at the vertex of the brace element at buckling.

moment along the length of the brace up to the location of the vertex is obtained as

$$m = \frac{x}{2}. \tag{3}$$

Substituting the values of M and m from Eqs. (1) and (3) into Eq. (2) and integrating, the incremental second order displacement, Δ_1, at the vertex of the brace is obtained as

$$\Delta_1 = 2\int_0^{L/2} \frac{2Pe}{EIL}\cdot\frac{x^2}{2}\,dx = \frac{PL^2e}{12EI}. \tag{4}$$

The kink or the eccentricity at the vertex of the brace now becomes $(e + \Delta_1)$. Assuming linear variation of the second order moments along the length of the brace, the following equilibrium state is reached for the transverse displacement, Δ_b, of the brace at buckling load, P_b:

$$\Delta_b = \frac{P_b L^2}{12EI}(e + \Delta_b). \tag{5}$$

Thus, from the above equation Δ_b is obtained as

$$\Delta_b = \left(\frac{\frac{P_b L^2}{12EI}}{1 - \frac{P_b L^2}{12EI}}\right)e. \tag{6}$$

When the axial load applied at the brace ends is equal to the buckling load, P_b, the second order moment at the vertex of the brace element is equal to the reduced plastic moment, M_{pb} of the brace as illustrated in Fig. 3e and f. Thus

$$(e + \Delta_b)P_b = M_{pb}. \tag{7}$$

Substituting Eq. (6) in Eq. (7), and solving for e, the initial eccentricity (or kink) that needs to be introduced in the middle of the brace to force it to buckle at an axial load, P_b is obtained as

$$e = \frac{M_{pb}}{P_b}\left(1 - \frac{P_b L^2}{12EI}\right). \tag{8}$$

The above equation is used to estimate the kink of the brace element used to model the cyclic axial behavior of braces using structural analysis programs capable of handling material and geometric nonlinearity.

6. Verification of proposed brace structural model

The analytical brace model described above is verified using the cyclic axial force-deformation results from experimental testing conducted on several braces made of box sections at the University of California, Berkeley [13]. The braces were tested by subjecting them to gradually increasing cyclic axial displacements. The descriptions of the test specimens and the analytical model as well as the comparison of the experimental and analytical results are given in the following sections.

6.1. Description of test specimens

The experimental test results from two box sections, which are named as Strut 18 and Strut 22 in [13] are used to verify the accuracy of the proposed brace model. Both box sections have a section size of TS4 × 4 × 1/2 in US customary units (TS102 × 102 × 12.7 in metric units) and a slenderness ratio of $\lambda = 80$. The braces are made of ASTM A501 steel with measured yield strength of 565 MPa. Thus, the yield axial force, P_y, for both box sections is 2320 kN. One of the brace specimens, which is referred to as Brace 1 throughout the text (Strut 22 in [13]), is 3.95 m long and has one end fixed and the other end pinned. The buckling

load of the brace is 1070 kN. The other brace specimen, which is referred to as Brace 2 throughout the text (Strut 18 in [13]), is 2.76 m long and its both ends are pinned. The buckling load of the brace is 1210 kN. The details of the test specimens are demonstrated in Fig. 4a.

6.2. Structural modeling

A 2D structural modal similar to the one presented in Fig. 2a is used in ADINA [9]. For Brace 1, a fixed support is introduced at one end of the brace member while a roller support is introduced at the other end. For Brace 2, a hinge support is introduced at one end of the brace member while a roller support is introduced at the other end. The value of the reduced plastic moment capacity, M_{pb}, of the box sections under the effect of the buckling load is obtained as 45 kN m for Brace 1 and 40 kN m for Brace 2 using the following equation that defines the axial force–moment interaction for steel box or "I" sections where the axial yield penetration, as per the derivation procedure in [11], is assumed to be limited to the web area:

$$M_{pb} = \left[1 - \left(\frac{P_b}{P_y}\right)^2 \frac{A^2}{8tZ}\right] M_p. \tag{9}$$

In the equation above, A, Z and t are respectively the cross-sectional area, plastic section modulus and the wall thickness of the box section and M_p is its plastic moment capacity without the presence of axial load. The value of M_{pb} obtained from Eq. (9), the buckling load and the brace properties are then substituted in Eq. (8) and the required eccentricity, e, of the structural model for Brace 2 is calculated as 11 mm. The eccentricity of Brace 1 is calculated as 21 mm following a trial and error procedure since Eq. (8) is not suitable for braces with a fixed end. In the trial and error procedure, first the structural model of a single brace member with a fixed and pinned end conditions is built. Then an eccentricity is assumed for the brace structural model. Next, a second order analysis under buckling load is conducted and the maximum second order bending moment is determined. This bending moment is then compared with the plastic bending moment, M_{pb}, of the box section. If the second order bending moment is not equal to, M_{pb}, the eccentricity is adjusted to achieve a second order bending moment equal to M_{pb} in the subsequent steps of the procedure. The calculated eccentricity is then used in the structural model for conducting the nonlinear cyclic analyses. It is worth mentioning that in most practical applications, the braces are assumed to be pin connected to the frame at both ends where Eq. (8) can easily be used for the calculation of e for modeling purposes.

The nonlinear properties of the brace members are defined as (i) a set of moment–curvature diagrams for various levels of axial loads and (ii) a stress–strain relationship for the box section. The moment–curvature diagrams of the box sections for axial load levels ranging between $P = 0$ and $P = 0.8P_y$ are obtained using a spread sheet program. The moment–curvature and axial stress–strain relationship for the box sections is presented in Fig. 4b and c. In the program, the box section is simulated using an

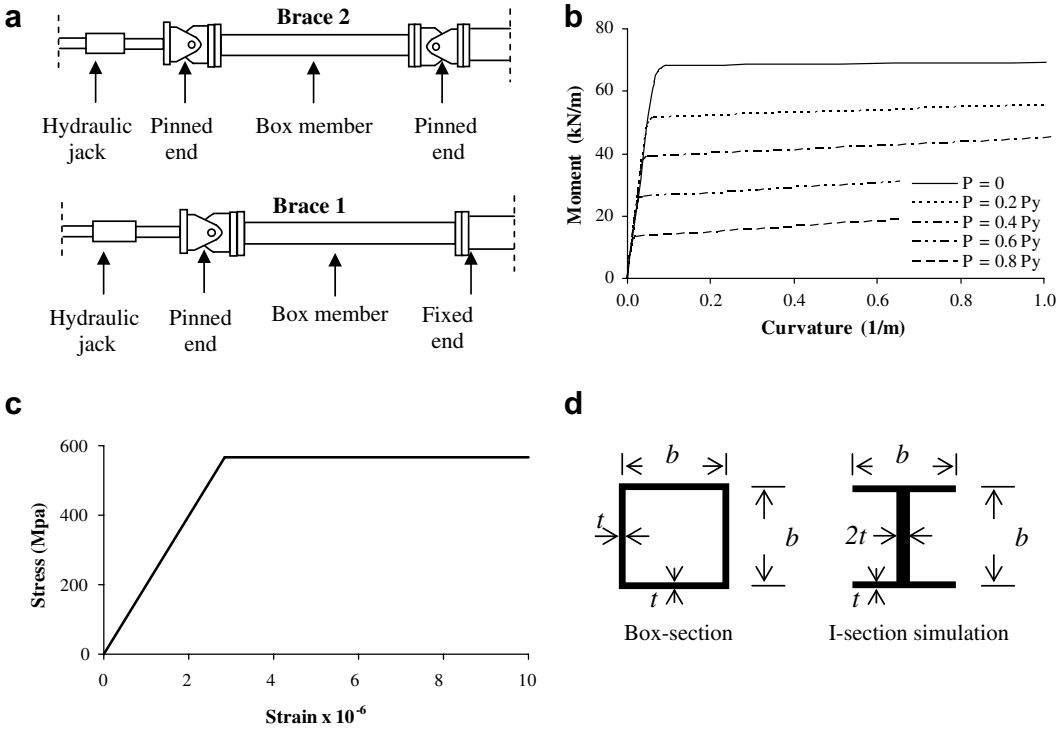

Fig. 4. Properties of box sections used for verification analytical model: (a) details of test specimens [12]; (b) moment–curvature relationships; (c) axial stress–strain relationship; (d) I-section simulation of box-section.

I-section bending about its strong axis. The thickness of the flanges of the I-section is set equal to those of the box section and the thickness of the web of the I-section is set equal to twice the thickness of one of the webs of the box section as demonstrated in Fig. 4d.

A cyclic static incremental axial displacement history is applied at the roller end of the braces, using the collapse analysis option with large displacement/rotation. The analysis results are discussed below.

6.3. Comparison of analytical and test results

Fig. 5a–d shows a comparison of the experimental [13] and analytical axial force–displacement hysteresis loops of the brace members considered in this study. From the comparison of the analytical and experimental results, it is clear that the general characteristics of the hysteresis loops of the analytical model are similar to those of the experimental model. Under a compressive axial load, buckling behavior is observed. Then, under each increasing cyclic negative (compressive) displacement step, there is a reduction in the compressive axial load capacity. Upon load reversal, a softening (stiffness degradation) behavior is also observed.

The total amount of energy dissipated for each one of the analytical and experimental results presented in Fig. 5a–d is calculated by summing up the areas under each force–displacement hysteresis loop using numerical integration. It is found that the maximum discrepancy between the total energy dissipated for the experimental and analytical hysteresis loops is roughly 15%. The accuracy of the shapes of the analytical hysteresis loops and the energy

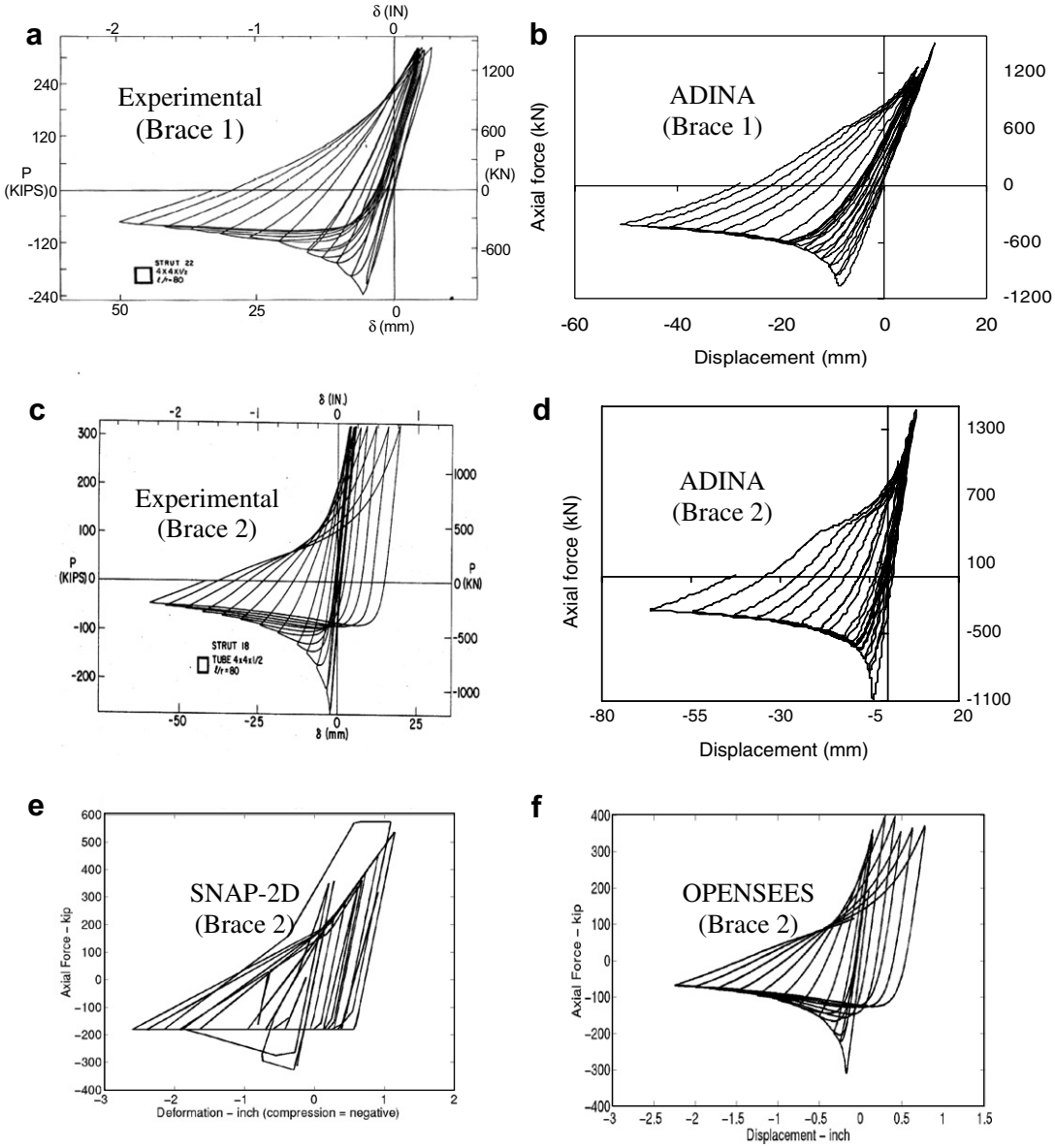

Fig. 5. Comparison of experimental [12] and analytical results for brace specimens: (a) test results for Brace 1; (b) ADINA results for Brace 1; (c) test results for Brace 2; (d) ADINA results for Brace 2; (e) SNAP-2D results for Brace 2 [8]; (f) OPENSEES results for Brace 2 [8].

dissipated compared to the experimental ones is believed to be satisfactory for analysis and design purposes in practice.

In addition, the analytical results for Brace 2 from two research oriented software, SNAP-2D (Fig. 5e) [8] and OPENSEES (Fig. 5f) [8] are compared with the experimental and analytical results presented in Fig. 5c and d. It is observed that the proposed analytical simulation technique used in commercially available software [9] produces results better than that of SNAP-2D and comparable to that of OPENSEES. This further reinforces the merits of the proposed technique for the simulation of the cyclic axial behavior of steel box sections using commercially available software.

7. Application to single story frames subjected to monotonic pushover displacements

The developed brace nonlinear structural model is used in a single-story, single-bay CBF with chevron braces to study the effect of the brace slenderness, brace axial stiffness and the beam's bending stiffness on the lateral behavior of the frame subjected to monotonic static pushover displacements at the top of the frame. A similar parametric study was conducted earlier by Khatib et al. [14] assuming pin connections between the beams and columns as in the case of a truss. However, in the present study, the connections between the beams and the columns are assumed to be rigid per the current state of practice. Thus, the effect of the brace and frame properties on the lateral load response of CBF is studied via a more realistic structural model including the effect of the rigid beam-column assembly on the overall response of the system.

7.1. Properties of the frame and the structural model

The single-story, single-bay frame and its structural model are demonstrated in Fig. 6a and b. The frame members are designed to have Class-I-sections per AISC (American Institute of Steel Construction) LRFD (Load and Resistance Factor Design) manual [1] to develop inelastic deformations without loss of capacity under lateral loading. The vertical support provided to the beam by the braces is neglected in the CBF as per the current state-of-design practice. The brace connections to the frame are assumed as pinned. The section sizes of the frame members are shown in Fig. 6a. In the structural model of the frame, the buckling capacity of the braces is calculated per AISC LRFD manual [1] and used in Eq. (8) together with other parameters to calculate the kinks of the braces shown in Fig. 6b. For the brace and other members of the frame, a set of moment–curvature and axial stress–strain relationships are obtained and defined to the program. An incremental static pushover displacement is applied at the upper node of the frame. The analyses results are discussed in the following sections.

7.2. Effect of brace slenderness

The effect of the brace slenderness on the lateral response of the CBF under monotonic lateral loading (or displacement) is demonstrated in Fig. 7a. The figure compares the static pushover analyses results of the frame for different brace slenderness values in the form of lateral displacement vs. base shear force. The change in the brace slenderness values is simulated by altering the eccentricity of the braces (Eq. (8)) to promote or delay buckling. The slenderness ratios considered are 40, 80 and 120. In addition to these, a hypothetical case is studied in which the buckling of the braces is prevented. In all the cases studied the axial elastic stiffness of the braces is kept constant.

It is observed from Fig. 7a that the compression brace buckles at the first step of the pushover analyses for all the slenderness ratios of 40, 80 and 120. This produces a sudden drop in the lateral force capacity of the frame. Following this, the lateral force capacity of the frame again picks up until the yield strengths of the other frame members are completely reached. Beyond that point, the post-elastic slope becomes negative, as the axial load capacity of the buckled brace keeps on decreasing with the lateral deformation of the frame as observed from Fig. 7b. Fig. 7a reveals that the brace slenderness has a major effect primarily on the elastic limit of the frame. CBF having braces with small slenderness has higher elastic limits. Consequently, such frames are unlikely to suffer any damage if subjected to low intensity ground motions. It is also observed that beyond the buckling point of the compression brace, the lateral force–displacement relationship, hence the energy absorption capacity, of the frame remains similar

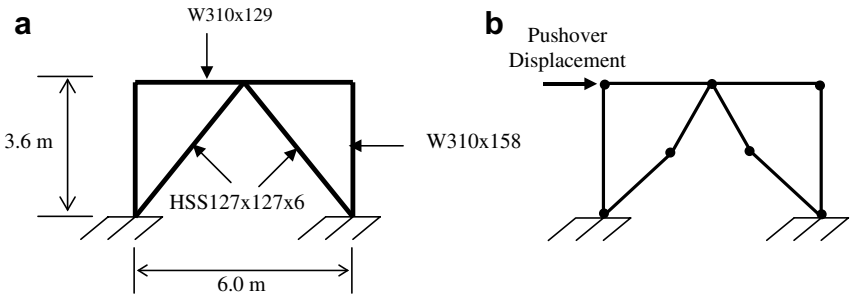

Fig. 6. (a) Single story frame; (b) structural model.

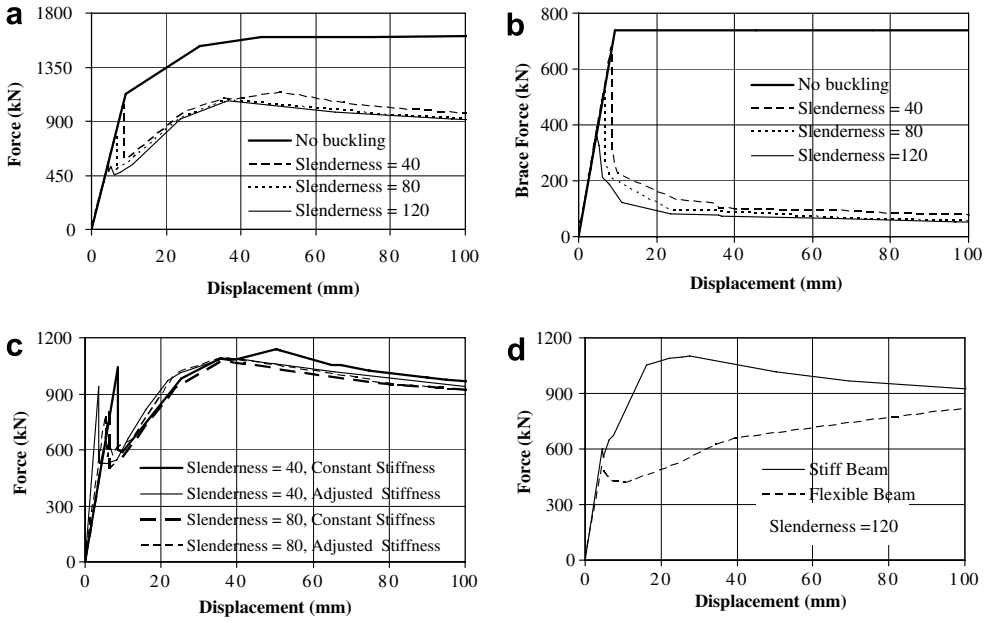

Fig. 7. (a) Lateral force–displacement relationship of frame for various brace slenderness ratios; (b) brace force vs. lateral frame displacement for various brace slenderness ratios; (c) lateral force–displacement relationship of frame for constant and adjusted brace stiffness; (d) lateral force–displacement relationship of frame for stiff and flexible beam.

regardless of the slenderness of the brace. Essentially, compared to the no buckling case (thick solid line in Fig. 7a), the primary effect of brace buckling is to reduce the energy absorption capacity and lateral stiffness of the frame dramatically. Therefore, buckling of the braces is likely to result in considerable damage to other frame components if the frame is subjected to high intensity ground motions.

7.3. Effect of brace stiffness

For all the slenderness ratios considered above, the axial elastic stiffness of the braces was kept constant. In this section, the effect of using the true elastic stiffness of the braces for each specific slenderness ratio is studied. The true elastic stiffness of the braces corresponding to a specific slenderness ratio is simulated (adjusted) by changing the modulus of elasticity of steel without altering the length of the braces in the structural model. The analyses results are presented in Fig. 7c. In the figure, the cases with constant and adjusted brace stiffness are compared. It is observed that the axial stiffness of the brace primarily affects the initial elastic slope of the force–displacement curve. The general behavior of the frames beyond the buckling point of the compression brace remains nearly unchanged regardless of the axial elastic stiffness of the brace since the buckling of the brace is mainly governed by its plastic behavior.

7.4. Effect of beam stiffness

In this section, the sensitivity of the CBF to the stiffness of the beam is studied. For this purpose, the flexural stiffness of the beam of the frame considered in the analyses is modified by a factor of 10 to obtain a flexible and a stiff beam. Fig. 7d displays lateral force–displacement relationship of the CBF for stiff and flexible beam cases for a brace slenderness ratio of 120. The figure displays a large difference in the lateral load capacity of the frame for the flexible and stiff beam cases. For a brace slenderness ratio of 120, the buckling load of the brace is very small compared to the yield force of the brace. Consequently, a large unbalanced vertical load on the beam will be produced due to the difference between the vertical components of the axial loads in the tension and compression braces. Thus, the flexible beam may be forced to displace down and may eventually reach its flexural yield capacity. This phenomenon produces a faster reduction in the axial load capacity of the compression brace [14] and hence a reduction in the lateral load capacity of the frame compared to the stiff beam case as observed from Fig. 7d. Thus, frames with stronger beams and with braces having larger buckling capacity are anticipated to have a superior behavior under lateral loading.

8. Application to single story frames subjected to seismic loads

In this section, nonlinear time history analyses of single-story, one-bay CBF are performed to determine whether the proposed brace model works under cyclic dynamic loading and to investigate the effects of various parameters on the seismic response of the CBF. The parameters studied are: (i) frequency characteristics and intensity of the ground motion; (ii) the percentage of frame (beams and

columns) vs. brace participation to lateral resistance of the CBF; (iii) slenderness ratio of the braces. The frame members considered for the static pushover analyses are redesigned to exhibit nonlinear behavior under seismic ground motions scaled to have peak ground accelerations ranging between 0.2 g and 0.5 g.

8.1. Ground motions considered for analyses

Ground motions are generally characterized by their peak ground acceleration to peak ground velocity (A_p/V_p) ratios [15,16] which represent their dominant frequency and energy content. Ground motions with intense long-duration acceleration pulses have low A_p/V_p ratios, whereas those with high frequency, short-duration acceleration pulses have high A_p/V_p ratios. Consequently, ground motions with various A_p/V_p ratios need to be considered to study the effect of the frequency characteristics of the ground motion on the seismic response of CBF. For this purpose, two sets of ground motions are considered. The first set consists of harmonic ground motions. The harmonic ground motions are particularly used to have a clear understanding of the effect of the frequency characteristics (A_p/V_p ratio) of the ground motion on the performance of the CBF. For the harmonic ground motions, $A_p/V_p = 2\pi/T_g$, where T_g is the excitation period of the harmonic wave. Harmonic ground motions with six A_p/V_p ratios ranging between 5.0 s^{-1} and 20.0 s^{-1} are considered for the analyses of the frames. Furthermore, the harmonic ground motions are scaled to have peak ground accelerations of 0.2 g, 0.3 g, 0.4 g and 0.5g representing small to large ground motion intensities. This is done to clearly understand the effect of the ground motion intensity on the performance of the frames.

The second set involves seven seismic ground motions with A_p/V_p ratios ranging between 5.5 s^{-1} and 21.5 s^{-1}. The seismic ground motions are scaled to have peak ground accelerations of 0.2 g, 0.35 g and 0.5 g representing respectively, small, moderate and large intensity earthquakes. The details of the seismic ground motions are presented in Table 1. These ground motions are used for examining the performance of the CBF as a function of the A_p/V_p ratio and A_p.

Table 1
Important features of earthquake records used in the analyses

Earthquake	Station	A_p (g)	V_p (cm/s)	A_p/V_p (1/s)
San Fernando, 1971	8244 Orion Blvd	0.13	23.9	5.5
Loma Prieta, 1989	Oakland Outer Wharf	0.22	35.4	6.1
Northridge, 1994	Arleta and Nordhoff Fire Station	0.34	40.4	8. 4
Imperial Valley, 1940	El Centro	0.35	32.3	10.6
Northridge, 1994	Santa Monica City Hall Grounds	0.37	24.9	14.6
Whitter Narrows, 1987	90079 Downey Birchdale	0.24	13.7	17.4
Parkfield, 1966	Cholame, Shandon	0.24	10.8	21.5

8.2. Proposed brace model under dynamic loading

In this section, the proposed brace model is tested under dynamic loading. For this purpose, the story drift vs. base shear hysteresis loop of the CBF subjected to a harmonic ground motion with $A_p/V_p = 6.28\ s^{-1}$and $A_p = 0.5$ g is displayed in Fig. 8. The figure exhibits the effects of the typical characteristics of the cyclic behavior of the brace on the seismic response of the CBF. On the compression side of the hysteresis loop, the effects of strength and stiffness degradation which are typical of buckling behavior of the brace are clearly observed. The softening of the frame stiffness associated with the cyclic behavior of the brace is also observed on the positive-displacement–negative-force region of the hysteresis loop. Thus, the proposed brace model appears to work under dynamic loading as well.

8.3. Effect of intensity and frequency characteristics of ground motion

In this section, the effect of the intensity and frequency characteristics of the ground motion on the seismic response of the CBF is investigated. Fig. 9a demonstrates the maximum story drift of the frame as a function of the A_p/V_p ratio of the harmonic ground motion for various ground motion intensities. Fig. 9b displays the same information for the seismic ground motions scaled to have various intensities. The figures reveal that at lower ground motion intensities, generally the CBF exhibits a stable seismic response regardless of the frequency characteristics or A_p/V_p ratio of the ground motion. However at higher ground motion intensities ($A_p = 0.5$ g) the response of the CBF is highly sensitive to the frequency characteristics or A_p/V_p ratio of the ground motion. Close examination of the behavior of the CBF under harmonic and seismic ground motions revealed that, the sensitivity of the frame's

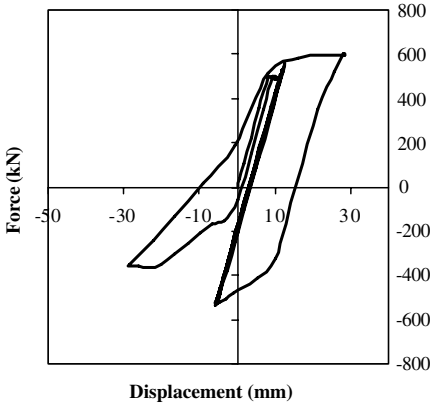

Fig. 8. Force–displacement hysteresis loop of the frame subjected to the harmonic ground motion with $A_p/V_p = 6.28\ s^{-1}$ and $A_p = 0.5$ g.

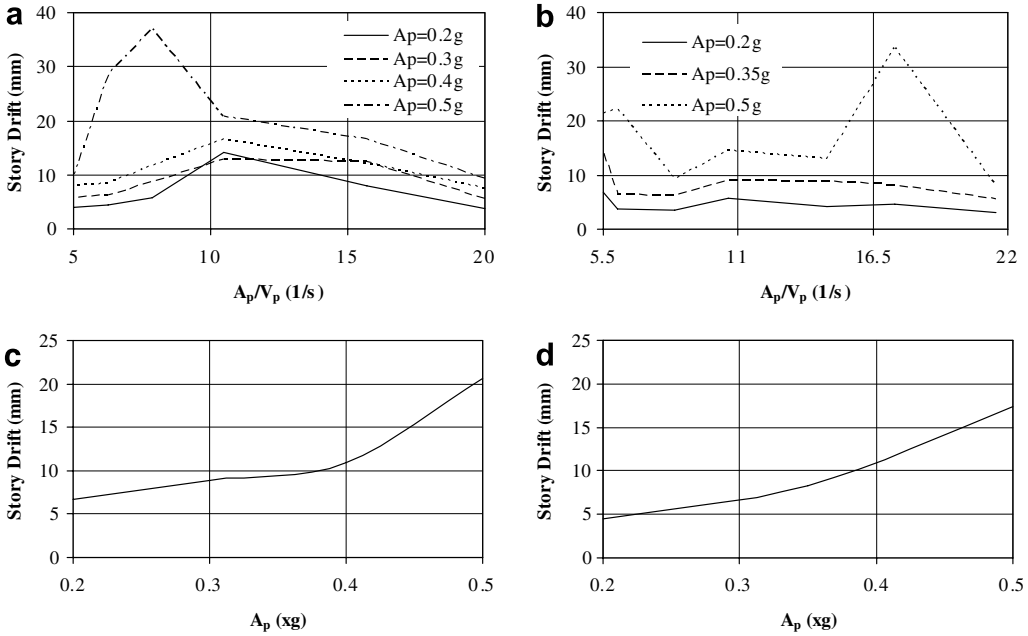

Fig. 9. (a) Story drift vs. A_p/V_p ratio of harmonic ground motions; (b) story drift vs. A_p/V_p ratio of seismic ground motions; (c) average story drift vs. intensity of harmonic ground motions; (d) average story drift vs. intensity of seismic ground motions.

seismic response to the frequency characteristics of the ground motion mainly depends on the buckling behavior of the brace. For seismic ground motions with lower intensities, either no buckling or limited buckling behavior of the brace is observed. This resulted in a more uniform response of the frame over the range of A_p/V_p ratios of the ground motions considered. However, for seismic ground motions with higher intensities, the buckling behavior of the brace becomes more dominant and the frame becomes more sensitive to the A_p/V_p ratio of the ground motion.

Fig. 9c displays the average of the maximum story drift of the frame for all the harmonic ground motions considered as a function of the peak ground acceleration of the harmonic ground motions. Fig. 9d displays the same information for the seismic ground motions. It is observed from the figures that the variation of the story drift as a function of the ground motion intensity is exponential. The story drift increases dramatically at higher ground motion intensities. This is again attributed to the buckling behavior of the braces. At higher ground motion intensities, the buckling behavior and hence strength and stiffness degradation of the frame becomes more dominant. Consequently, the frame exhibits very large story drifts.

Further examination of the behavior of the CBF revealed that the frame's satisfactory response at low to medium ground motion intensities is a result of two important factors: (i) the relatively stocky braces with a slenderness, $\lambda = 96$, minimize the detrimental effect of the buckling behavior of the braces that is generally associated with more slender braces; (ii) the presence of the relatively strong frame members (beam and columns) demotes the effect of the buckling behavior of the braces (the braces constitute only 40% of the lateral strength of the frame). Nevertheless, for higher intensity ground motions ($A_p = 0.5$ g) the maximum drifts of the CBF become significant since the other members of the CBF (beam and columns) also reach their yield capacity allowing the buckling of the braces to dominate the behavior.

8.4. Effect of frame versus brace participation and brace slenderness

In the previous section, it is observed that the CBF generally exhibits a good response for small to medium intensity ground motions due to the presence of relatively strong frame members and stocky braces. Thus, in this section, the effect of the brace participation and the slenderness of the braces on the seismic response of the CBF are investigated.

To carry out the study, three frames, namely Frame 1, 2 and 3 are considered. Frame 1 is the one already studied in the previous sections where the beams and columns constitute 60% and the braces constitute 40% of the lateral strength of the CBF. The slenderness of the braces in this frame is 96. In Frame 2, the braces resist 60% of the lateral load applied to the CBF. The slenderness ratio of the braces is the same as that of Frame 1. Frame 3 is similar to Frame 2 but, the slenderness ratio of the braces is 125.

The analyses results are presented in Fig. 10 in the form of graphs between A_p/V_p and the story drift for different intensities of seismic ground motions considered in this study. It is observed that for $A_p = 0.2$ g and 0.35 g, the CBF generally yields a good response regardless of the properties of the frame for the range of frame contribution (40–60%) and brace slenderness ratios (96 and 125) considered in this study. Obviously, since the brace participation

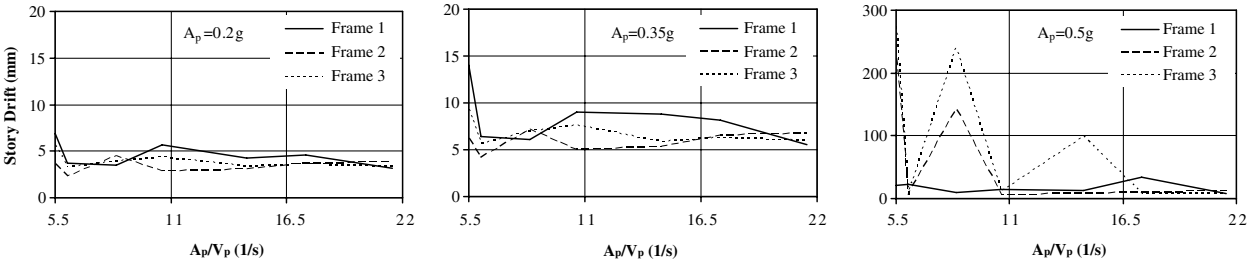

Fig. 10. Comparison of story drifts for CBF with various properties as a function of the A_p/V_p ratio of seismic ground motions for $A_p = 0.2$ g, 0.35 g and 0.5 g.

to the lateral strength of the frame is smaller in Frame 1 (40%) the story drift for this frame is larger than those of the other two frames.

For $A_p = 0.5$ g, Frames 2 and 3 produce exceptionally higher drifts compared to that of Frame 1. This may be attributed to the more dominant buckling behavior of the braces resulting from the larger brace contribution to the overall lateral strength of the CBF in Frames 2 and 3. It is also observed that the story drift of Frame 3 is even higher in comparison to Frame 2 due to the presence of braces with larger slenderness ratios in Frame 3. Furthermore, the seismic response becomes more sensitive to the A_p/V_p ratio of the ground motion for Frames 2 and 3 as observed from the humps and undulations displayed in Fig. 10.

Thus, it may be concluded that the contribution of the brace to the overall strength of the frame and the slenderness of the brace are important factors affecting the seismic response of a CBF. The seismic performance of CBF with larger brace contribution and brace slenderness is poor when subjected to high intensity ground motions.

9. Conclusions

A nonlinear structural model is developed as part of this study to simulate the nonlinear cyclic behavior of steel box section braces including their buckling behavior using commercially available structural analysis software capable of handling material and geometric nonlinearity. The developed brace model is verified using available test results. It is found that the accuracy of the shapes of the analytical hysteresis loops and the energy dissipated compared to the experimental ones is satisfactory for analysis and design purposes in practice. The proposed brace model is also implemented in a single-story, single-bay CBF and subjected to a harmonic ground motion. The lateral force–displacement hysteresis loop of the frame exhibited the typical effects of brace cyclic behavior on the overall response of the frame. Thus, the proposed brace model may be used for the nonlinear static and dynamic analysis and design of CBF.

The developed nonlinear brace model is then used to study the effect of various ground motion and structural parameters on the seismic response of single story, single bay CBF with chevron braces. The analyses results revealed that although the brace slenderness has a major effect on the elastic limit of the frame, its effect on the post buckling behavior is insignificant. Essentially, the primary effect of brace buckling is to reduce the energy absorption capacity and lateral stiffness of the frame dramatically. Furthermore, investigation of the effect of the beam stiffness on the lateral response of the CBF revealed that frames with stronger beam and with braces having larger buckling capacity have a superior behavior under lateral loading. Moreover, it is found that at higher ground motion intensities, the story drift becomes significant and the response of the CBF becomes highly sensitive to the frequency characteristics of the ground motion due to the buckling behavior of the braces. It is also found that the seismic performance of CBF with larger brace contribution and brace slenderness is poor when subjected to high intensity ground motions.

Acknowledgement

The authors thank ADINA R&D Inc. for providing the ADINA software to Bradley University for conducting the research presented in this paper.

References

[1] AISC. Manual of steel construction, load and resistance factor design. Chicago, IL: American Institute of Steel Construction; 2001.
[2] BSSC. NEHRP recommended provisions for the development of seismic regulations for new buildings and other structures, Federal Emergency Management Agency, Washington, DC; 2000.
[3] ICC. International building code. Falls Church, Virginia: International Code Council; 2000.
[4] Jain AK, Goel SC. Inelastic cyclic behavior of bracing members and seismic response of braced frames of different proportions. Report No.: UMEE78R3, University of Michigan, Ann Arbor, MI; 1978.
[5] Ikeda K, Mahin SA. Refined physical theory model for predicting the seismic behavior of braced steel frames. Report No.: UCB/EERC-84/12, Earthquake Engineering Research Center, University of California, Berkeley, CA; 1984.
[6] Rai D, Goel SC, Firmansjah J. SNAP-2DX – a general purpose computer program for static and dynamic nonlinear analysis of 2-D structures: User's guide, Department of Civil and Environmental Engineering, University of Michigan, Ann Arbor, Michigan; 1995.
[7] Jin J, El-Tawii S. Inelastic cyclic model for steel braces. ASCE J Eng Mech 2003;129(5):548–57.

[8] Mahin SA, Uriz P. Seismic performance assessment of special concentrically braced steel frames. In: Proc of international workshop on steel and concrete composite constructions, National Center for Research on Earthquake Engineering (NCREE), Taiwan; 2003. p. 1–15.
[9] ADINA Automatic dynamic incremental nonlinear analysis, Version 8.2, ADINA R&D, Inc., Watertown, MA; 2004.
[10] Bathe KJ. Finite element procedures. New Jersey: Prentice Hall; 1996.
[11] Bruneau M, Uang C-M, Whittaker A. Ductile design of steel structures. New York, NY: McGraw Hill; 1997.
[12] Gere JM, Timoshenko SP. Mechanics of materials. Boston, MA: PWS; 1984.
[13] Black RG, Wenger WA, Popov EP. Inelastic buckling of steel struts under cyclic load reversal. Report No: UCB/EERC-80/40, Earthquake Engineering Research Center, University of California, Berkeley, CA; 1980.
[14] Khatib IF, Mahin SA, Pister KS. Seismic behavior of concentrically braced steel frames. Report No: UCB/EERC-88/01, Earthquake Engineering Research Center, University of California, Berkeley, CA; 1988.
[15] Kramer SL. Geotechnical earthquake engineering. New Jersey, USA: Prentice Hall; 1996.
[16] Dicleli M, Buddaram S. Effect of isolator and ground motion characteristics on the performance of seismic-isolated bridges. Earthquake Eng Struct Dyn 2006;35(2):233–50.